Influence of local-field effects upon the optical properties of trigonal selenium

Kenneth G. Hamilton
Department of Physics, University of California, San Diego, La Jolla, California 92093
(Received 24 March 1986)

The dielectric function of selenium was calculated from first principles, including local-field effects in both the random-phase approximation and Hartree-Fock formulations. The requisite inversion of an infinitely large matrix was performed by transforming to finite matrices which span Wannier functions. The appearance of excitonic effects leads to a possible mechanism for photoconductivity.

I. INTRODUCTION

When an external electric field is applied to a real substance, an internal redisposition is known to take place which generates a polarization field; the sum of the external field and the polarization is the actual field which is observed inside the material. The most basic treatment of local-field effects considers each atom as a simple dipole, exhibiting a linear response to the field surrounding it. This method results in the standard Lorenz-Lorentz formula.[1-3]

These assumptions survive in the traditional view of many-body effects, that such effects are long-lived, with little or no interaction between them. This leads to the specification of physical properties in terms of linear-response functions which produce elementary excitations of matter in response to small external perturbations using the quantum field theory formalism,[4,5] and then evaluated according to a number of different assumptions.

The dielectric tensor function, defined as the inverse ratio of the total electric field to the externally applied field, is one of these linear-response functions. The dielectric is an appropriate vehicle for the study of the many-body effects of electrons in solids; from it, such other properties as optical loss and reflectivity can be readily evaluated. Microscopically, the polarization field is due to various deformations of the electronic clouds surrounding the nuclei. The significance of this is that the internal redistribution of charge is not a uniform reaction, nor one which simply follows the wavelength of the applied field, but rather it varies markedly on the scale of the atoms and crystalline cells of the substance.

In fact, if a crystal is excited by an external field of wave vector $\mathbf{q}$, then the periodicity of the lattice will give rise to microscopic fields of $\mathbf{q}+\mathbf{G}$, where $\mathbf{G}$ represents all of the reciprocal lattice vectors. Quantum field theory provides the definition for the dielectric matrix, whose components span a space of reciprocal-lattice vectors. Calculation of an observable dielectric function requires that this infinite-dimensional matrix be formally inverted, after which a limiting process is taken for small external wavevector. The problem of the inversion has been a stumbling block in this process.

The inversion can be done using the method of Hanke and Sham,[6,7] which involves transforming the matrix into a finite-dimensional space, spanned by Wannier functions. In this way, the most important interaction terms are included in the smaller matrices, from which the terms which have less importance are neglected. Then the electron-electron correlation potential can be included as a straightforward operation. This effect, which is conventionally known as the random phase approximation,[8,9] or "RPA," is equivalent to the time-dependent Hartree approximation. Using the matrix formulation, it is relatively simple to extend the RPA treatment[10] to include exchange effects; the extended RPA treatment then is equivalent to the time-dependent Hartree-Fock approximation.

Standard theoretical treatments, such as the empirical pseudopotential method,[11] attempt to fit the gaps of their calculated band structure to the locations of the peaks which are seen in optical experiments. When a dielectric function is computed from such a fitted band structure, invariably the strengths of the transitions disagree with the experiments to which the band structures were fitted. In particular, the theoretical dielectric functions always show too much strength at high energies, and not enough at low ones.

The observation has been made[6,12] that inclusion of local-field correlation in the RPA worsens the comparison between theory and experiment, but that when both correlation and exchange effects are used the agreement is greatly improved. This is also the case when the inversion is done by directly inverting large finite subsets of the dielectric matrix.[13] The problem of the incorrect weighting of the dielectric function transitions is seen primarily in group-IV elements, and compounds of types III-V and II-VI.

The treatment of diamond by Hanke and Sham showed the time-dependent Hartree-Fock approximation to be a substantial improvement over both the RPA and noninteracting models. Because trigonal selenium can be viewed as a collection of parallel chains, this one dimensionality can be expected to produce an even stronger local-field effect. Pressure-dependent reflectivity measurements[14] suggest that substantial local-field effects exist in selenium, although pseudopotential calculations purport to show that these results are caused by interchain interactions.[15]

II. DESCRIPTION OF SELENIUM

Selenium has outer electron shells of $4s^2 4p^4$; it thus behaves chemically like sulfur and tellurium. It crystallizes into several forms, only one of which, the trigonal structure, is treated here. Trigonal selenium is composed of spiral chains of atoms, with three atoms making up each turn of the helix (each turn is a unit cell). In a crystal, many chains are stacked together in parallel to form a hexagonal superlattice, as shown in Fig. 1. Such a crystal can be described by the space group D_3^4; the enantiomorph D_3^6 also exists, but only the former will be treated. The angle formed by the two chain bonds on each site is 105°, which can cause the lattice to look almost cubic from another direction. Figure 2 shows the Brillouin cell for this structure.

In hexagonal coordinates, the positions of successive members of a chain are $(u,0,0)$, $(-u,-u,\frac{1}{3})$, $(0,u,\frac{2}{3})$, etc. The dimension of a unit cell in the z direction (down the chain) is $c_0 = 4.949\,45$ Å, while the distance between the center of one chain and its nearest neighbor is $a_0 = 4.355\,17$ Å, with the radius of the spiral being $u = 0.217 a_0$. It can be calculated that the nearest-neighbor distance within a chain is 2.324 09 Å, while the minimum interchain atom-to-atom distance is 3.467 14 Å; this difference can justify using a model in which interchain bonding is ignored.

It is possible to take advantage of the spiral chain structure to calculate energy bands using a one-dimensional model,[16,17] in which the 105° bond angle is treated as a perturbation on a 90° case. Such calculations basically produce bands which are fairly flat, although they do show the symmetry point Z as being the location of the minimum direct gap between valence and conduction bands. In the most straightforward models,[16,17] the gap comes out to be significantly larger than 2 eV, however.

Trigonal selenium has long been known for its strong photoconductivity in the visible (2–2.5 eV) region; by way of contrast, the amorphous form shows only a very weak effect. Photon absorption measurements with photovoltaic cells of trigonal selenium have indicated that the minimum energy absorption edge is actually due to indirect transitions.[18] A three-dimensional (3D) band structure calculation,[19] using the Korringa-Kohn-Rostoker method,[20] indicated that the minimum gap is at symmetry point H, as did an empirical pseudopotential calculation.[21] Reflectivity measurements[22] have been only partially successful in assigning observed features to points in the Brillouin zone, leading to the belief that a number of exciton-assisted interactions are present.

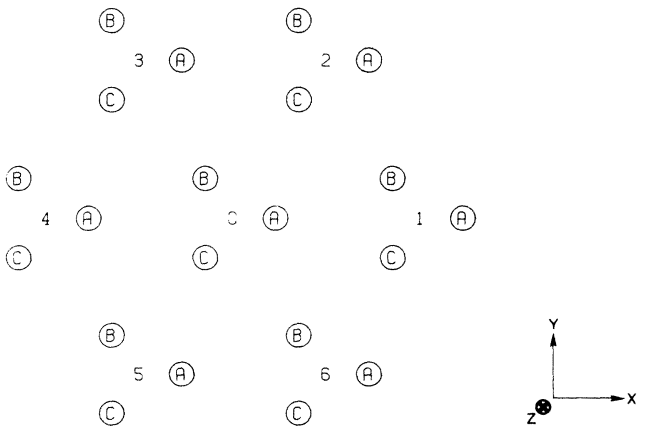

FIG. 1. The trigonal selenium lattice, viewed down the chain axis.

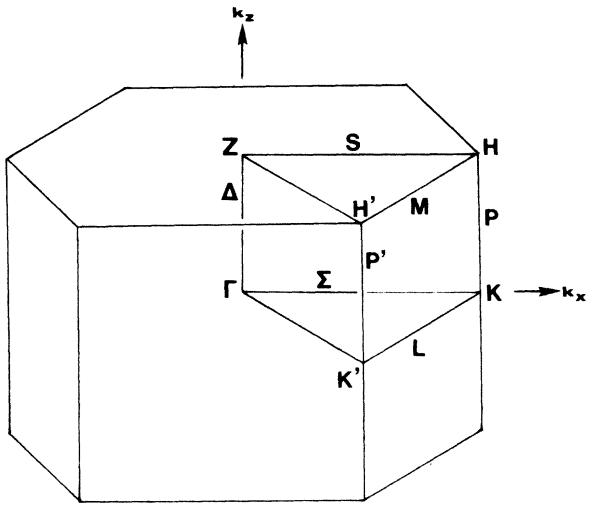

FIG. 2. The Brillouin zone for trigonal selenium.

Irradiation of crystals with lasers produce numerous photoluminescent spectral lines, which have been ascribed to excitonic decay,[23] a conclusion which has also been made by measurement of the reflectivity near the band edge,[24] based upon Urbach's law.[25] Optical absorption experiments[26] indicate that indirect transitions are observed when the applied electric field is parallel to the chain axis of a crystal, while an exciton accounts for the exponential tail observed when the electric field is in the perpendicular direction. Measurements of electroreflectance[27] report five excitons between 1.8 and 3.2 eV.

Temperature-dependent electroabsorption experiments[28] lead to the conclusion that the minimum transition takes place from the valence band at H to the conduction band at Z, using Elliot's theory of indirect transitions.[29] Large scale orthogonalized plane wave calculations have also been reported,[30,31] but they include some strange results, including a minimum direct gap of only 1.0 eV. A small calculation of local-field corrections has been done by Nizzoli.[32,33] Unfortunately, his work was restricted to the case of a static ($\omega = 0$) applied field, and was directly inverted in subsets of the reciprocal-lattice space. His results did, however, indicate that inclusion of local-field effects is essential for calculation of a dielectric constant which reproduces experiment.

III. ATOMIC ORBITAL MODELS AND INTEGRALS

In 1950, Boys[34] proposed the use of functions of the form $x^l y^m z^n \exp(-\alpha r^2)$ to compose the basis set for

molecular calculations. The formulation lends itself to particularly simple analytic results.[35] Many integrals can be obtained for s orbitals, and then differentiated to produce similar quantities for orbitals of higher angular momentum. In this system, the elementary functions

$$\varphi_0(\mathbf{r};\alpha)=\exp(-\alpha r^2) \tag{3.1}$$

and

$$\varphi_i(\mathbf{r};\alpha)=r_i\exp(-\alpha r^2) \tag{3.2}$$

can be used to make up s and p orbitals as the linear superpositions

$$\phi_0(\mathbf{r})=\sum_{I=1}^{N} G_I\varphi_0(\mathbf{r};\alpha_I) \tag{3.3}$$

and

$$\phi_i(\mathbf{r})=\sum_{I=1}^{N} G_I\varphi_i(\mathbf{r};\alpha_I)\ , \tag{3.4}$$

respectively. The calculation of overlap integrals between two s orbitals on different sites is a fairly simple task; since the elementary functions are related by

$$\varphi_i(\mathbf{r}-\mathbf{A};\alpha)=\frac{1}{2\alpha}\frac{\partial}{\partial A_i}\varphi_0(\mathbf{r}-\mathbf{A};\alpha)\ , \tag{3.5}$$

it follows that the overlap between two p orbitals can be obtained by two partial derivatives of the s case. Important matrix elements, including those involving the position vector $\mathbf{r}$ and the Laplacian operator ∇^2, can be conveniently produced in close form. The general four-center potential integral,

$$V=\int\int \phi(\mathbf{r}-\mathbf{A})\phi(\mathbf{r}-\mathbf{B})v(\mathbf{r}-\mathbf{r}') \times\phi(\mathbf{r}'-\mathbf{C})\phi(\mathbf{r}'-\mathbf{D})d^3r\,d^3r' \tag{3.6}$$

can also be calculated by means of a rapidly convergent numerical procedure, for both s and p orbitals.

IV. BAND THEORY

Consider a "nearly cubical" crystal, in which three p-type orbitals reside on each atomic site, and in which three sites make up each unit cell. The sites within the cell can be labeled as $s=A,B,C$. The vector which connects A to B can be designated $\mathbf{R}_\mu$, the vector from B to C can be called $\mathbf{R}_\nu$, and the vector which runs from site C in one cell to site A of the next cell may be referred to as $\mathbf{R}_\lambda$. This arrangement is shown in Fig. 3. These vectors are related to the conventional Cartesian coordinate system if we specify that the axis of the selenium chain runs along z; then

$$\mathbf{R}_\mu+\mathbf{R}_\nu+\mathbf{R}_\lambda=\mathbf{c}=(0,0,c_0)\ . \tag{4.1}$$

Since μ, ν, and λ are orthogonal axes, we can use them for the directions of the atomic orbitals, which we can call p_μ, p_ν, and p_λ, just as though we were dealing with p_x, p_y, and p_z. Then sites A and B are connected by one strong σ bond, which we call $p_\mu p_\mu\sigma$, and by two weaker π bonds, $p_\nu p_\nu\pi$ and $p_\lambda p_\lambda\pi$. Since there are three types of atomic wave functions on each of three sites, there must

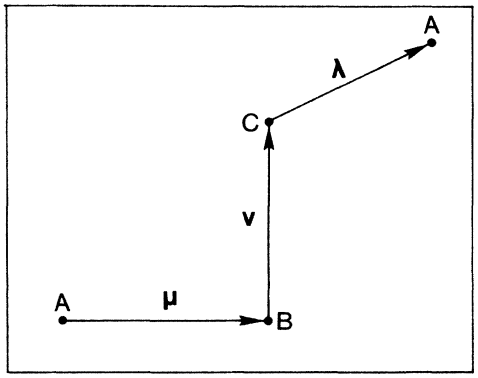

FIG. 3. Naming scheme for the interatomic bonds.

be nine distinct energy bands. The band wave functions are given by the Bloch formulation,

$$\psi_{bk}(\mathbf{r})=N^{-1/2}\sum_{j,s,\alpha} C_{b\alpha s}(\mathbf{k})\exp(i\mathbf{k}\cdot\mathbf{r}_j)\phi_\alpha(\mathbf{r}-\mathbf{r}_{js})\ , \tag{4.2}$$

where $b=1,2,3,\ldots,9$ enumerates the bands.

Schrödinger's equation takes the form of

$$H^{j'j}_{\alpha's',\alpha s}-E_{bk}S^{j'j}_{\alpha's',\alpha s}=0\ , \tag{4.3}$$

where

$$H^{j'j}_{\alpha's',\alpha s}=\int\phi^*_{\alpha'}(\mathbf{r}-\mathbf{r}_{j's'})H\phi_\alpha(\mathbf{r}-\mathbf{r}_{js})d^3r \tag{4.4}$$

and

$$S^{j'j}_{\alpha's',\alpha s}=\int\phi_{\alpha'}(\mathbf{r}-\mathbf{r}_{j's'})\phi_\alpha(\mathbf{r}-\mathbf{r}_{js})d^3r\ . \tag{4.5}$$

Given that on each side there is a local Schrödinger's equation,

$$[-\tfrac{1}{2}\nabla^2+v(\mathbf{r})]\phi_\alpha(\mathbf{r})=E_a\phi_\alpha(\mathbf{r})\ , \tag{4.6}$$

which is governed by an atomic energy parameter E_a, we find that

$$H^{j'j}_{\alpha's',\alpha s}=2E_aS^{j'j}_{\alpha's',\alpha s}+\tfrac{1}{2}\Delta^{j'j}_{\alpha's',\alpha s} \tag{4.7}$$

when certain terms are ignored, where $\Delta^{j'j}_{\alpha's',\alpha s}$ is the matrix element of the Laplacian operator, of a form similar to Eq. (4.4). Because of the use of Boys-type orbitals, the members of S and Δ can readily be given values.

Assuming only nearest-neighbor interactions, Eq. (4.3) becomes a 9×9 matrix problem. If the rows and columns are arranged in the order

$$\alpha s=\mu A,\mu B,\mu C,\nu B,\nu C,\nu A,\lambda C,\lambda A,\lambda B\ ,$$

then the problem breaks down into three 3×3 blocks. The k_x and k_y dependence of the problem can be removed by a unitary rotation, leaving the energy eigenvalue problem dependent only upon k_z. Because of the block-diagonal form of the problem, each of the three threefold degenerate energy bands is simply given as a solution of a cubic equation; the eigenvector coefficients can then be

TABLE I. Orbital parameters for model I.

i	α_i	G_i
1	62.8545	25.155 572
2	3.6523	−2.171 301
3	0.2551	0.232 335
4	0.015	0.002 462

obtained as a solution of simultaneous equations.

We will define and use two separate sets of orbital parameters, $\{\alpha_i, G_i\}$. The first set ("model I") was chosen so as to produce a direct gap of approximately 2.6 eV; this allows the model to conform to the observation that selenium has its lowest-energy response in the visible region. A set of parameters which satisfy these requirements are those specified in Table I. The overlap values, and matrix elements of position, and Laplacian and Hamiltonian operators which derive from this model are listed in Table II, with energies given in Hartrees. The atomic energy used in the computation of the Hamiltonian matrix elements is −6.5 eV. The resulting band structures for model I are shown in Fig. 4, while Fig. 5 displays the relative amplitudes of the $k=0$ wave vectors on the three sites making up a unit cell.

Clementi and Roetti[36] have calculated isolated-atom electronic wave functions in the Roothaan-Hartree-Fock approximation. Their results were expressed in terms of sums of Slater functions to various levels of complexity. The radial component of their most comprehensive solution is used as an ideal to which a Boys-type orbital wave function was fitted. The parameters specified in Table III provide the fit shown in Fig. 6, which will be called "model II." When this model is used to calculate matrix elements, the results are as shown in Table IV, and atomic energy of −8 eV is assumed. Figure 7 shows the energy bands calculated from this model: As can be seen, the direct gap is a startling 9.4 eV, a substantial variance from the generally accepted value of 2—3 V.

TABLE II. Integral values from model I: overlaps (S), and matrix elements of position (X), Laplacian operator (Δ), and Hamiltonian (H), for same-site (0), sigma bond (σ) and pi bond (π). Δ and H are in units of hartrees.

$S_0=1.0$
$S_\sigma=-0.167\,813\,4$
$S_\pi=0.224\,926\,2$
$X_0=0.0$
$X_\sigma=-0.368\,509\,1$
$X_\pi=0.493\,925\,5$
$\Delta_0=-5.327\,700$
$\Delta_\sigma=0.180\,317\,9$
$\Delta_\pi=-0.017\,833\,32$
$H_0=-0.238\,882\,8$
$H_\sigma=0.170\,334\,4$
$H_\pi=-0.116\,378\,7$

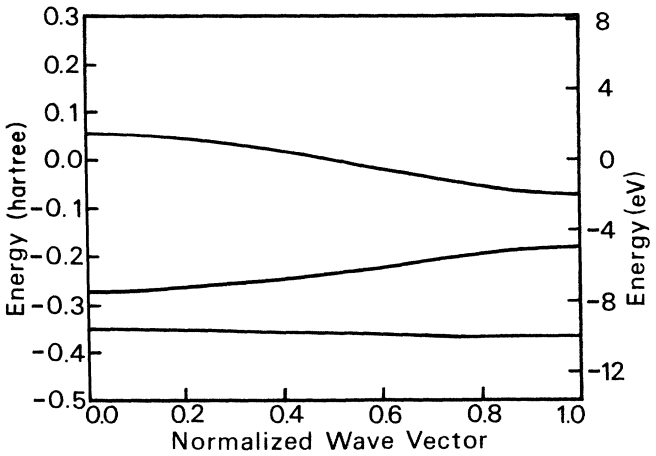

FIG. 4. The energy-band structure of model I.

V. DERIVATION OF THE DIELECTRIC TENSOR

A. Separation of the irreducible polarizability

Many-body theory provides us with a definition for the proper polarizability, $\tilde{\chi}$, which allows us to write the dielectric matrix as

$$\epsilon(\mathbf{q}+\mathbf{G},\mathbf{q}+\mathbf{G}',\omega)=\delta_{\mathbf{G},\mathbf{G}'}-v(\mathbf{q}+\mathbf{G})\tilde{\chi}(\mathbf{q}+\mathbf{G},\mathbf{q}+\mathbf{G}',\omega)\ , \tag{5.1}$$

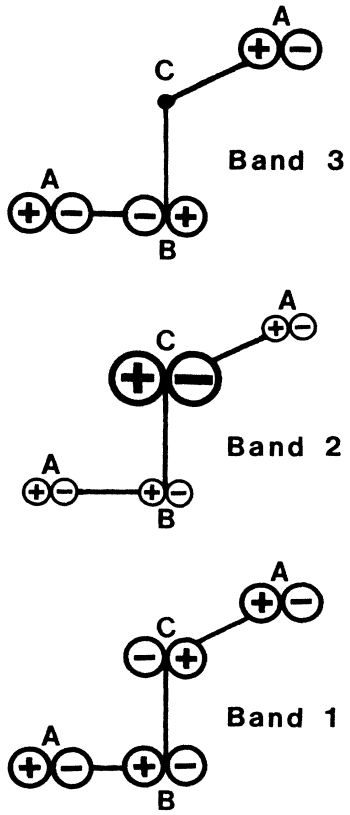

FIG. 5. Relative amplitudes for bands 1, 2, and 3, at $k_z=0$.

TABLE III. Orbital parameters for model II.

i	α_i	G_i
1	62.8545	20.428 91
2	3.6523	−1.763 32
3	0.2551	0.188 68
4	0.1	0.026 33

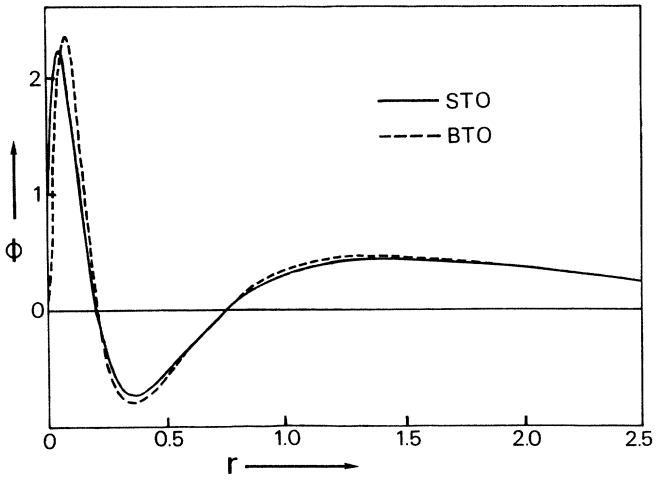

FIG. 6. Comparison between radial parts of the Clementi-Roetti $4p$ Slater-type orbital ("STO") and the Boys-type orbital ("BTO") of model II.

where $v(\mathbf{q})=4\pi e^2/q^2\Omega_0$ is the ordinary Coulomb potential, and Ω_0 is the volume of a unit cell. Equation (5.1) includes the reciprocal lattice vectors $\mathbf{G}$ and $\mathbf{G}'$, which make it possible to describe Umklapp scattering. The inverse dielectric matrix is ϵ^{-1}, which has the property

$$\sum_{\mathbf{K}} \epsilon(\mathbf{q}+\mathbf{G},\mathbf{q}+\mathbf{K},\omega)\epsilon^{-1}(\mathbf{q}+\mathbf{K},\mathbf{q}+\mathbf{G}',\omega)=\delta_{\mathbf{G},\mathbf{G}'} . \tag{5.2}$$

If the inverse dielectric matrix can be obtained, then the limiting process

$$\epsilon(\omega)=\lim_{\mathbf{q}\to 0}\frac{1}{\epsilon^{-1}(\mathbf{q},\mathbf{q},\omega)} \tag{5.3}$$

when applied to the $\mathbf{G}=\mathbf{G}'=\mathbf{0}$ term produces the observable dielectric function. The various elements of the familiar 3×3 dielectric tensor are obtained by taking the limit as the wave vector goes to zero from different directions. The major hurdle to calculation is the inversion of ϵ to ϵ^{-1}, since both are $\infty\times\infty$ matrices.

If Eq. (5.1) is postmultiplied by ϵ^{-1}, and the inner sum taken, then we obtain a recursive definition for the inverse dielectric matrix,

$$\epsilon^{-1}(\mathbf{q}+\mathbf{G},\mathbf{q}+\mathbf{G}',\omega)=\delta_{\mathbf{G},\mathbf{G}'}+\sum_{\mathbf{K}} v(\mathbf{q}+\mathbf{G})\tilde{\chi}(\mathbf{q}+\mathbf{G},\mathbf{q}+\mathbf{K},\omega)\epsilon^{-1}(\mathbf{q}+\mathbf{K},\mathbf{q}+\mathbf{G}',\omega) . \tag{5.4}$$

When this relation is inserted into itself repeatedly, the result (summations being assumed) is

$$\epsilon^{-1}=\delta+v\tilde{\chi}+v\tilde{\chi}v\tilde{\chi}+v\tilde{\chi}v\tilde{\chi}v\tilde{\chi}+\cdots . \tag{5.5}$$

The polarization due to Bloch waves is

$$\tilde{\chi}(\mathbf{q}+\mathbf{G},\mathbf{q}+\mathbf{G}',\omega)=\sum_{\substack{b_1,b_2,b_3,b_4\\ \mathbf{k},\mathbf{k}'}} \langle b_2,\mathbf{k}\,|\,\exp[-i(\mathbf{q}+\mathbf{G})\cdot\mathbf{r}]\,|\,b_1,\mathbf{k}+\mathbf{q}\rangle X(b_1,\mathbf{k}+\mathbf{q};b_2,\mathbf{k};b_3,\mathbf{k}';b_4,\mathbf{k}'+\mathbf{q};\mathbf{q},\omega)$$
$$\times\langle b_4,\mathbf{k}'+\mathbf{q}\,|\,\exp[i(\mathbf{q}+\mathbf{G}')\cdot\mathbf{r}]\,|\,b_4,\mathbf{k}'\rangle \tag{5.6}$$

TABLE IV. Integral values from model II.

$S_0=1.0$
$S_\sigma=-0.370\,844\,0$
$S_\pi=0.176\,688\,5$
$X_0=0.0$
$X_\sigma=-0.814\,353\,1$
$X_\pi=0.387\,998\,2$
$\Delta_0=-3.809\,853$
$\Delta_\sigma=0.272\,682\,2$
$\Delta_\pi=-0.043\,913\,57$
$H_0=-0.292\,933\,0$
$H_\sigma=0.353\,606\,1$
$H_\pi=-0.125\,472\,8$

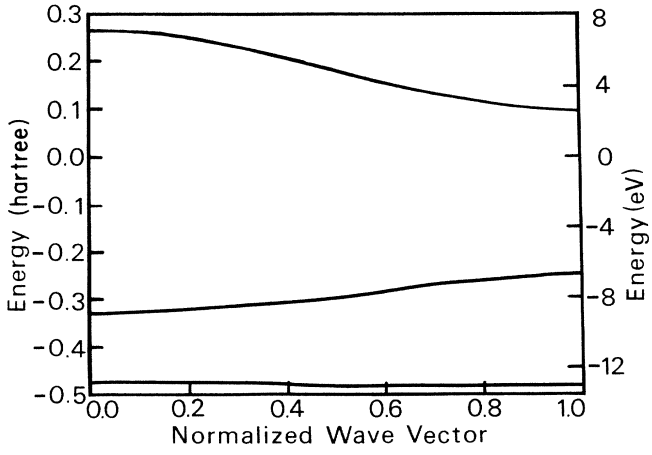

FIG. 7. The energy-band structure of model II.

where the bands are numbered by the b_i indexes. The first matrix element in Eq. (5.6) is then

$$\langle b_2,\mathbf{k}\,|\,\exp[-i(\mathbf{q}+\mathbf{G})\cdot\mathbf{r}]\,|\,b_1,\mathbf{k}+\mathbf{q}\rangle=\sum_{\alpha_1,s_1,\alpha_2,s_2,J} C^*_{b_2s_2\alpha_2}(\mathbf{k})C_{b_1s_1\alpha_1}(\mathbf{k}+\mathbf{q})\exp[i(\mathbf{k}+\mathbf{q})\cdot\mathbf{R}_j]A_{\alpha_1s_1\alpha_2s_2J}(\mathbf{q}+\mathbf{G}) , \tag{5.7}$$

with $J=j_1-j_2$, and introducing the function

$$A_{\alpha_1s_1\alpha_2s_2J}(\mathbf{q})=\int \exp(-i\mathbf{q}\cdot\mathbf{u})\phi^*_{\alpha_2}(\mathbf{u}-\mathbf{R}_{s_2})\phi_{\alpha_1}(\mathbf{u}-\mathbf{R}_{s_1}-\mathbf{R}_J)d^3u . \tag{5.8}$$

Defining the polarizability core as

$$N_{pp'}(\mathbf{q},\omega)=\sum_{\substack{b_1,b_2,b_3,b_4\\ \mathbf{k},\mathbf{k}'}} C^*_{b_2s_2\alpha_2}(\mathbf{k})C_{b_1s_1\alpha_1}(\mathbf{k}+\mathbf{q})\exp[-i(\mathbf{k}+\mathbf{q})\cdot\mathbf{R}_J]$$
$$\times X(b_1,\mathbf{k}+\mathbf{q};b_2,\mathbf{k};b_3,\mathbf{k}';b_4,\mathbf{k}'+\mathbf{q};\mathbf{q},\omega)\exp[-i(\mathbf{k}'+\mathbf{q})\cdot\mathbf{R}_{J'}]C^*_{b_4s_4\alpha_4}(\mathbf{k}'+\mathbf{q})C_{b_3s_3\alpha_3}(\mathbf{k}') , \tag{5.9}$$

where $p\equiv\{\alpha_1,s_1,\alpha_2,s_2,J\}$, $p'\equiv\{\alpha_4,s_4,\alpha_3,s_3,J'\}$, then we have the polarizability recast as

$$\tilde{\chi}(\mathbf{q}+\mathbf{G},\mathbf{q}+\mathbf{G}',\omega)=\sum_{p,p'} A_p(\mathbf{q}+\mathbf{G})N_{pp'}(\mathbf{q},\omega)A^*_{p'}(\mathbf{q}+\mathbf{G}') . \tag{5.10}$$

Equation (3.5) then becomes

$$\epsilon^{-1}=\delta+vANA^*+vANA^*vANA^*+vANA^*vANA^*vANA^*+\cdots=\delta+vASA^* , \tag{5.11}$$

with the modified polarizability core being defined by

$$S=N(I-VN)^{-1} \tag{5.12}$$

and $V=A^*vA$ is the correlation potential matrix, which has the explicit form

$$V_{pp'}(\mathbf{q})=\sum_m \exp(-i\mathbf{q}\cdot\mathbf{R}_m)\int d^3r\int d^3r'\,\phi_{\alpha_2}(\mathbf{r}-\mathbf{R}_{s_2}-\mathbf{R}_m)\phi^*_{\alpha_1}(\mathbf{r}-\mathbf{r}_{s_1}-\mathbf{R}_J-\mathbf{R}_m)$$
$$\times v(\mathbf{r}-\mathbf{r}')\phi^*_{\alpha_3}(\mathbf{r}'-\mathbf{R}_{s_3})\phi_{\alpha_4}(\mathbf{r}'-\mathbf{R}_{s_4}-\mathbf{R}_{J'}) . \tag{5.13}$$

The aggregate indices p and p' point to sites and orbitals. We can, and do, choose to sum only over nearest-neighbor sites. When we do this, we have effectively reduced the infinite matrices to finite size in a manner which retains the dominant terms and drops off the less-significant portions. This provides a definition for ϵ^{-1} in which the inversion of Eq. (5.12) can be performed in place of the massive one indicated by Eq. (5.2).

The polarizability function, X, in Eq. (5.6) is given, in the RPA or time-dependent Hartree approximation by

$$X^{\mathrm{RPA}}(b_1,\mathbf{k}+\mathbf{q};b_2,\mathbf{k};b_3,\mathbf{k}';b_4,\mathbf{k}'+\mathbf{q};\mathbf{q},\omega)\simeq\delta_{\mathbf{k}\mathbf{k}'}\delta_{b_1b_4}\delta_{b_2b_3}X_0(b_1,\mathbf{k}+\mathbf{q};b_2,\mathbf{k};\omega) , \tag{5.14}$$

where

$$X_0(b_1,\mathbf{k}+\mathbf{q};b_2,\mathbf{k};\omega)=\frac{2}{N}\frac{f_{b_1\mathbf{k}+\mathbf{q}}-f_{b_2\mathbf{k}}}{E_{b_1\mathbf{k}+\mathbf{q}}-E_{b_2\mathbf{k}}-\omega-i0} , \tag{5.15}$$

where $E_{b\mathbf{k}}$ and $f_{b\mathbf{k}}$ are single-electron energy and occupation numbers for the Bloch state $(b,\mathbf{k})$.

B. The Hartree-Fock (HF) approximation

Fermion exchange is produced by using the Bethe-Salpeter relation, which takes the form

$$X^{\mathrm{HF}}(b_1,\mathbf{k}+\mathbf{q};b_2,\mathbf{k};b_3,\mathbf{k}';b_4,\mathbf{k}'+\mathbf{q})=X^{\mathrm{RPA}}(b_1,\mathbf{k}+\mathbf{q};b_2,\mathbf{k};b_3,\mathbf{k}';b_4,\mathbf{k}'+\mathbf{q})$$
$$-\frac{1}{2}\sum_{\substack{b_5,b_6,b_7,b_8\\ \mathbf{k}'',\mathbf{k}'''}} X^{\mathrm{RPA}}(b_1,\mathbf{k}+\mathbf{q};b_2,\mathbf{k};b_5,\mathbf{k}'';b_6,\mathbf{k}''+\mathbf{q})$$
$$\times v^x(b_6,\mathbf{k}''+\mathbf{q};b_5,\mathbf{k}'';b_7,\mathbf{k}''';b_8,\mathbf{k}'''+\mathbf{q})$$
$$\times X^{\mathrm{HF}}(b_8,\mathbf{k}'''+\mathbf{q};b_7,\mathbf{k}''';b_3,\mathbf{k}'';b_4,\mathbf{k}'+\mathbf{q}) \tag{5.16}$$

using the exchange potential

$$v^x(b_6,\mathbf{k}''+\mathbf{q};b_5,\mathbf{k}'';b_7,\mathbf{k}''';b_8,\mathbf{k}'''+\mathbf{q})=\int d^3r\int d^3r'\,\psi^*_{b_6\mathbf{k}''+\mathbf{q}}(\mathbf{r})\psi_{b_5\mathbf{k}''}(\mathbf{r}')v(\mathbf{r}-\mathbf{r}')\psi_{b_7\mathbf{k}'''}(\mathbf{r}')\psi_{b_8\mathbf{k}'''+\mathbf{q}}(\mathbf{r})\ . \tag{5.17}$$

The Hartree-Fock polarizability core can then be described in terms of the RPA one by

$$N^{\mathrm{HF}}_{pp'}(\mathbf{q},\omega)=N^{\mathrm{RPA}}_{pp'}-\frac{1}{2N}\sum_{p_1,p_2}N^{\mathrm{RPA}}_{pp_1}(\mathbf{q},\omega)V^x_{p_1p_2}(\mathbf{q})N^{\mathrm{HF}}_{p_2p'}(\mathbf{q},\omega) \tag{5.18}$$

using the exchange potential matrix

$$V^x_{pp'}(\mathbf{q})=\sum_m\exp(-i\mathbf{q}\cdot\mathbf{R}_m)\int d^3r\int d^3r'\,\phi_{\alpha_2}(\mathbf{r}'-\mathbf{R}_{s_2}-\mathbf{R}_m)\phi_{\alpha_1}(\mathbf{r}-\mathbf{R}_{s_1}-\mathbf{R}_J-\mathbf{R}_m)$$
$$\times v(\mathbf{r}-\mathbf{r}')\phi^*_{\alpha_3}(\mathbf{r}'-\mathbf{R}_{s_3})\phi_{\alpha_4}(\mathbf{r}-\mathbf{R}_{s_4}-\mathbf{R}_{J'})\ . \tag{5.19}$$

Inclusion of exchange effects can thus be produced by revising Eq. (5.12) to become

$$S=N[I-(V-V^x)N]^{-1}\ . \tag{5.20}$$

C. The limit of small wave vector

The inverse dielectric function can be written as

$$\epsilon^{-1}(\mathbf{q}+\mathbf{G},\mathbf{q}+\mathbf{G}',\omega)=\delta_{\mathbf{G}\mathbf{G}'}+v(\mathbf{q}+\mathbf{G})\chi(\mathbf{q}+\mathbf{G},\mathbf{q}+\mathbf{G}',\omega)\ , \tag{5.21}$$

where

$$\chi(\mathbf{q}+\mathbf{G},\mathbf{q}+\mathbf{G}',\omega)=\tilde{\chi}(\mathbf{q}+\mathbf{G},\mathbf{q}+\mathbf{G}',\omega)+\sum_{\mathbf{K}}\tilde{\chi}(\mathbf{q}+\mathbf{G},\mathbf{q}+\mathbf{K},\omega)v(\mathbf{q}+\mathbf{K})\chi(\mathbf{q}+\mathbf{K},\mathbf{q}+\mathbf{G}',\omega)\ . \tag{5.22}$$

Ambegaoker and Kohn[37] defined $\hat{\chi}$ as the sum of all polarization processes not involving the long-range part of the Coulomb interaction,

$$\hat{\chi}(\mathbf{q}+\mathbf{G},\mathbf{q}+\mathbf{G}',\omega)=\tilde{\chi}(\mathbf{q}+\mathbf{G},\mathbf{q}+\mathbf{G}',\omega)+\sum_{\mathbf{K}\ (\neq 0)}\tilde{\chi}(\mathbf{q}+\mathbf{G},\mathbf{q}+\mathbf{K},\omega)v(\mathbf{q}+\mathbf{K})\hat{\chi}(\mathbf{q}+\mathbf{K},\mathbf{q}+\mathbf{G}',\omega)\ . \tag{5.23}$$

Kohn[30] also showed that, for insulating crystals, $\tilde{\chi}(\mathbf{q},\mathbf{q},\omega)$ is proportional to q^2 as $q\to 0$. Equation (5.23) provides the same property to $\hat{\chi}$, so that we have

$$\hat{\chi}(\mathbf{q},\mathbf{q},\omega)=\hat{\chi}^{(2)}(\omega)q^2+O(q^4)\ . \tag{5.24}$$

The two functions χ and $\hat{\chi}$ are related by

$$\chi(\mathbf{q},\mathbf{q},\omega)=\hat{\chi}(\mathbf{q},\mathbf{q},\omega)/[1-v(\mathbf{q})\hat{\chi}(\mathbf{q},\mathbf{q},\omega)]\ . \tag{5.25}$$

In light of this, we find that

$$\frac{1}{\epsilon^{-1}(\mathbf{q},\mathbf{q},\omega)}=1-v(\mathbf{q})\hat{\chi}(\mathbf{q},\mathbf{q},\omega) \tag{5.26}$$

so that, in the limit as $q\to 0$, we have

$$\epsilon(\omega)=1-\hat{\chi}^{(2)}(\omega)4\pi e^2/\Omega_0\ . \tag{5.27}$$

D. Three dielectric formulations

We can, at this point, define three methods of defining the dielectric functions. In the simplest, we completely ignore local-field effects by assuming that all of the off-diagonal ($\mathbf{G}\neq\mathbf{G}'$) elements of the dielectric matrix are zero. The inversion of a diagonal matrix is trivial, and the dielectric function attains the definition

$$\bar{\epsilon}_{\eta\eta'}(\omega)=1-\frac{4\pi e^2}{\Omega_0}\sum_{p,p'}f^\eta_pN_{pp'}(\omega)f^{\eta'}_{p'}\ , \tag{5.28}$$

where

$$f^\eta_p=\int\rho_\eta\phi^*_{\alpha_2}(\boldsymbol{\rho}-\mathbf{R}_{s_2})\phi_{\alpha_1}(\boldsymbol{\rho}-\mathbf{R}_{s_1}-\mathbf{R}_J)d^3\rho\ , \tag{5.29}$$

with η being one of the principal axes of the crystal. This definition is arrived at by taking the limit for small wave vector of $A(\mathbf{q})$.

The next order of approximation consists of including the correlation, but leaving out the exchange potential, so that

$$\epsilon^{\mathrm{RPA}}_{\eta\eta'}=1-\frac{4\pi e^2}{\Omega_0}\sum_{p,p'}f^\eta_pS_{pp'}(\omega)f^{\eta'}_{p'}\ , \tag{5.30}$$

with $S(\omega)$ being defined by Eq. (5.12) in the $q\to 0$ limit.

Finally, in the full Hartree-Fock approximation, the dielectric is again given by Eq. (5.30), but with $S(\omega)$ defined by the small wave vector limit of Eq. (5.20). It should be noted that terms of the f vector are matrix elements of position, calculable by the methods described in Sec. III, and that in the $q\to 0$ limit, the potential matrices of Eqs. (5.13) and (5.19) are integrals of the form given in Eq. (3.6) and are also easily computed due to our orbital formulation.

VI. IMPLEMENTATION OF THE SOLUTION

For the purposes of actually computing the dielectric functions, the problem was broken into three phases: (a) calculation of the potential matrices V and V^x, (b) evaluation of the Hartree polarizability core N, and (c) production of the final dielectric functions. These phases were carried out by three separate computer programs. When the potential matrices are analyzed in detail, it turns out that there are only 24 distinct four-center integrals in which the centers are actually located on only one or two sites. These values are independent of ω, and so were calculated first.

The Hartree polarizability core is defined as the $q \rightarrow 0$ limit of Eq. (5.9), when Eqs. (5.14) and (5.15) are substituted. Because of the manner in which the band structure was set up, especially the analytic handling of the k_x and k_y dependence, the summation over kk' collapses into a single one-dimensional integral over k_z. The integration was performed, for each value of ω, by a numerical procedure based on Simpson's rule. Detailed inspection of the terms of the polarizability core matrix was used to limit the calculation to only the unique terms, which were all computed to the same accuracy.

The third major program was used to effect the matrix multiplications and inversions implied by Eqs. (5.12), (5.20), (5.28), and (5.30), thus resulting in the three dielectric functions $\bar{\epsilon}$, ϵ^{RPA}, and ϵ^{HF}. The functions were calculated for values of energy from 0 to 2 hartrees, in steps of 0.05.

VII. OPTICAL SPECTRUM OF SELENIUM

It appears that the best experimental data for comparison of the theoretical results is by Bammes *et al.*,[38] who measured optical reflectivity at near normal incidence using synchrotron radiation. Their procedures were conducted using a strongly polarized source; as a result they were able to observe that trigonal selenium has distinct differences when the incident radiation is polarized parallel and perpendicular to the chain axis. They measured reflectance from bulk selenium crystals, and from that, then calculated dielectric functions in both principal directions.

Figure 8 shows the imaginary part of the parallel dielectric function for the model I theory (indicated for the three calculational methods by different symbols), compared to experiment. The dielectric with no local-field effects included shows its first peak in the 3-eV region, but does not come anywhere near to matching the strength indicated by experiment. The $\bar{\epsilon}$ results also exhibit peaks in the 8—10 eV area, which generally match the location of a couple of experimental response peaks, although the theoretical numbers are much too high.

The RPA theory shows a small, sharp response in the 3-eV region, but the most noticeable change from $\bar{\epsilon}$ is the increase in strength of the higher energy peaks. When exchange terms are included, the strength is shifted down in energy considerably, with the greatest response being at 2 eV; this is the same phenomenon which has been observed in silicon.[6]

The real part of the dielectric function is shown in Fig. 9. While demonstrating, generally, the same shifts in strengths as the imaginary part does, this calculation leads to an explanation of Nizzoli's observation[32,33] that exchange interactions boost the value of the static dielectric constant, and seem to be necessary to obtain agreement with experiment. Our shifting down of strengths and his static increase are thus the same. Figures 10 and 11 display the imaginary and real parts of the dielectric function for model I in the direction perpendicular to the chain axis. The shifting up of strength in the RPA and sliding down in Hartree-Fock are again seen. It is interesting to note that the major response of the HF curve occurs at an experimental peak, but not at the largest one.

A comparison of the imaginary parallel model II calculations to the experimental data is visible in Fig. 12. It can be seen that, in the absence of local-field effects, there is no response below the direct gap of 9 eV, with the major response lying between 15 and 20 eV. When correlation effects only are included, the 9 eV peak is sharpened, but another, more substantial response occurs in the area

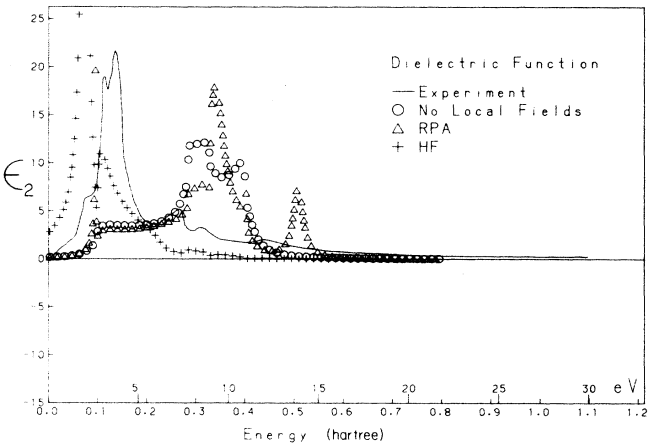

FIG. 8. The imaginary part of the parallel dielectric function for model I.

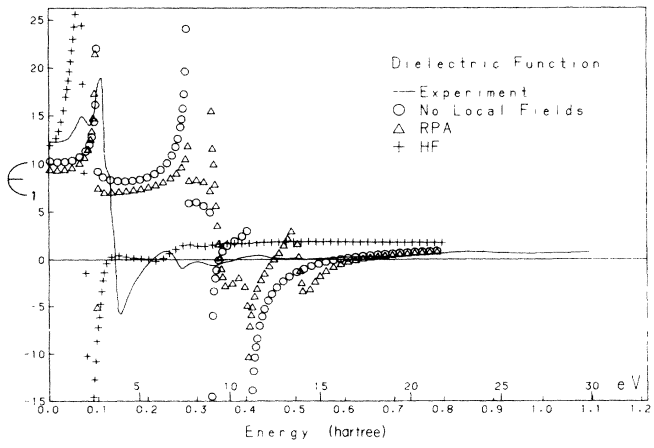

FIG. 9. The real part of the parallel dielectric function for model I.

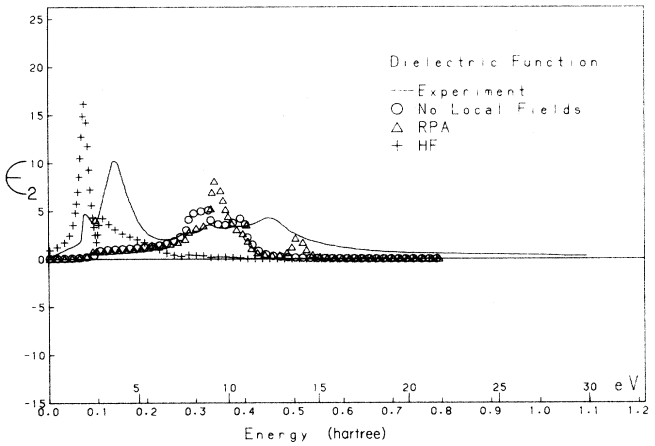

FIG. 10. The imaginary part of the perpendicular dielectric function for model I.

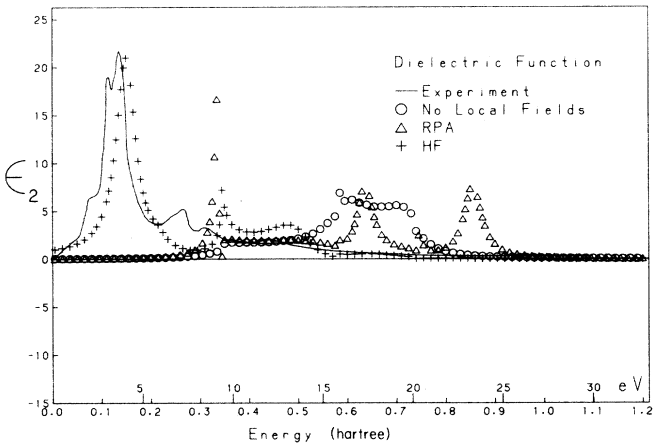

FIG. 12. The imaginary part of the parallel dielectric function for model II.

of 24 eV. Remarkable agreement with experiment is achieved when both correlation and exchange potentials are used. Then the largest peak in the HF calculation occurs at about 4 eV, where it matches very closely in location and strength; an additional two peaks are at 9 and 13 eV, where they generally match a pair of experimental responses.

The real part of the parallel dielectric function appears in Fig. 13. As before, the HF computation yields the best agreement with the major response, although the strength in the 7—12 eV regime is high. Figures 14 and 15 demonstrate the dielectric function in the perpendicular direction. The now-expected shifting of strengths occur, even though th HF calculation predicts a strength of the major peak which is somewhat low.

VIII. DISCUSSION

In both models I and II excitonic response (below the direct gap) dominates the Hartree-Fock results. The nature of these excitons seems to differ somewhat from those which are ordinarily encountered in other materials.

These are two types of excitons which are recognized by solid state theory. The Frenkel exciton[39] is highly localized, and is best regarded as an excited state of a single atom; typically, it can show a binding energy of several electron volts. A Wannier exciton,[40] on the other hand, extends over a large area of space, several times the interatomic distance of the crystal. Because of this relatively large distance between the electron and its hole partner, a Wannier exciton customarily has a binding energy of only a fraction of an electron volt. The atomic system which was used here contained no information about any electron states other than the $4p$ ones. Thus, the creation of a true Frenkel exciton was not possible. On the other hand, the binding energies seen for the calculated excitons is much too large for a traditional Wannier exciton.

The normal derivation of a Wannier exciton begins by assuming that the electrical field within the crystal is uniform throughout, so that the electrons and holes can see one another over large distances. This, of course, is the exact opposite of the situation which we are assuming to

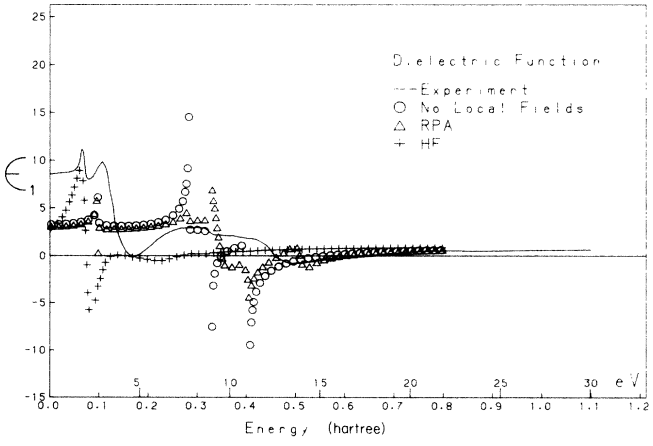

FIG. 11. The real part of the perpendicular dielectric function for model I.

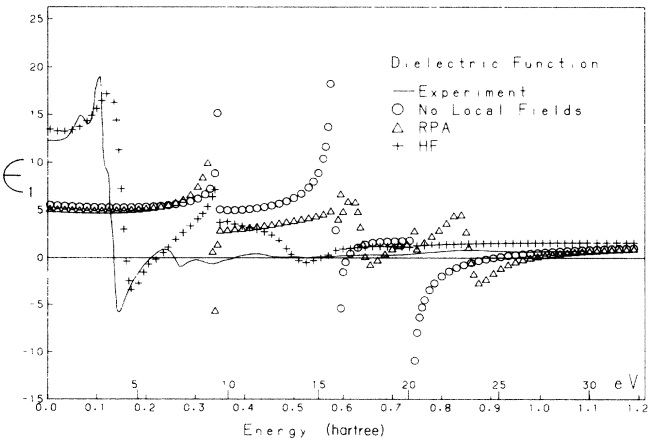

FIG. 13. The real part of the parallel dielectric function for model II.

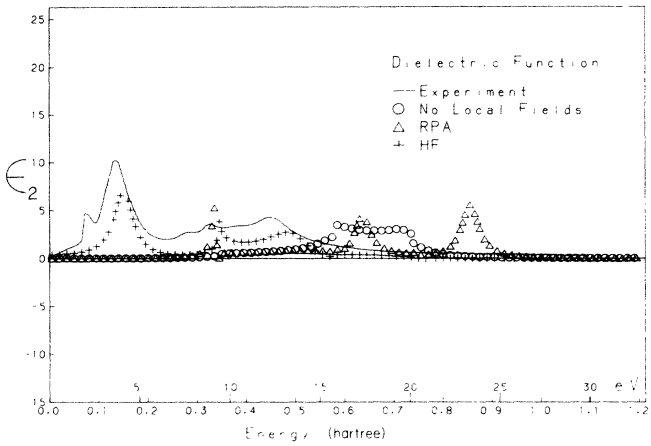

FIG. 14. The imaginary part of the perpendicular dielectric function for model II.

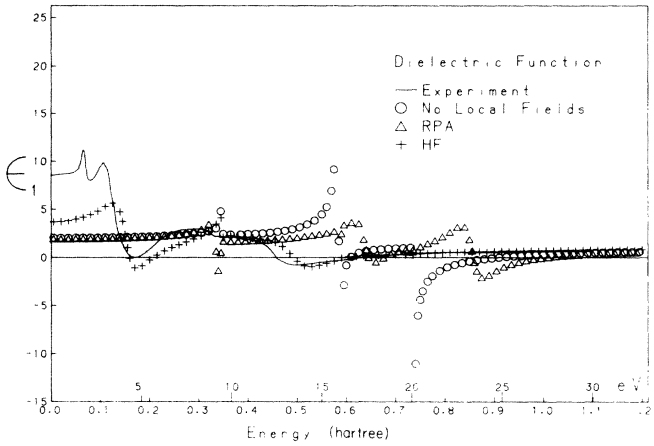

FIG. 15. The real part of the perpendicular dielectric function for model II.

be the case in selenium. Instead of a flat electric potential, we have presumed the existence of a strongly varying one. Since a crystal has a regular lattice structure, and the fields generated by the nuclei and orbitals are emplaced in this regular pattern, it follows that the electric field has a periodic behavior over space. If the local-field effect is strong, then this periodic disturbance consists of major areas of high potential and substantial lows. This situation should make it possible for those electrons which are bound into excitons to travel around in the valleys of potential energy, while their partner holes move in the high-potential areas. This is a situation in which the excitons can be rather strongly bound: In fact, the binding energy of the excitons should be a good indication of the magnitude of the inhomogeneities in the electric potential.

The kind of exciton which we have generated in the theoretical calculations may best be thought of as a highly modified form of Wannier exciton, in which the bound pair is mobile within the crystal. Experimentally, a situation similar to this has been observed[41] in the absorption spectrum of thin films of inert gasses, where excitons of a nature between Frenkel and Wannier types were present. The same phenomenon has been seen[42] in the cubic semiconductors CuBr and ZnSe.

An objection can be raised to the fact that the lowest-energy peak in the selenium theory is excitonic in nature. Surely, one can argue, there must be some sort of a true interband transition in the visible (2—3 eV) region, since selenium is a well-known photoconductor. An exciton, being neutral, cannot carry charge, and therefore a band-to-band transition is required to explain the photoconductivity. It seems, however, that photoconductivity can be produced by excitons. The mechanism goes as follows: Suppose that light produces an exciton, which is mobile and travels until it encounters a defect in the lattice, where it becomes trapped. While there, the exciton is collided with by a second exciton, which decays, providing the energy to free the original electron and hole. An alternative mechanism would involve absorption of a second photon by the exciton, with the same result, an unbound pair. This type of phenomenon was observed a number of years ago[43] in Cu_2O and CdS (a useful photoconductor, if there ever was one) and also[44] in ZnS. The existence of excitons in Cu_2O has also been observed.[45]

A highly convincing argument for excitonically produced photoconductivity comes from Gross and Novikov[46] who observed that all crystals which have a complex absorption edge structure (as would be expected in the presence of Wannier excitons) are strong photoconductors, while similar crystals which do not have excitons exhibit very little photoconductivity. As examples of the first group, they point to Cu_2O, CdS, CdSe, ZnS, HgI, PbI_2, and AgI; for the second class of crystals, they cite MoO_3, BiO_3, V_2O_5, As_2S_3, and yellow PbO. In particular, they point to HgI_2, which has two modifications: the red form has exciton lines and a strong photoeffect, while in the yellow form, the exciton lines are missing and so, for all practical purposes, is photoconductivity.

ACKNOWLEDGMENTS

The author takes pleasure in thanking Professor Lu Sham for many enlightening discussions during the progress of this work. This article was based on a dissertation submitted in partial fulfillment of the requirements for the Ph.D. degree at the University of California, San Diego.

[1]Stephan L. Adler, Phys. Rev. **126**, 413 (1962).
[2]Nathan Wiser, Phys. Rev. **129**, 62 (1963).
[3]H. Ehrenreich and M. H. Cohen, Phys. Rev. **115**, 786 (1959).
[4]A. A. Abrikosov, L. P. Gorkov, and I. E. Dzyalozhinski, *Methods of Quantum Field Theory in Statistical Physics* (Prentice-Hall, Englewood Clifs, 1963).
[5]N. H. March, W. H. Young, and S. Sampanthar, *The Many-Body Problem in Quantum Mechanics* (Cambridge University Press, Cambridge, 1967).
[6]W. Hanke and L. J. Sham, Phys. Rev. B **12**, 4501 (1975).

[7]W. Hanke, Adv. Phys. **27**, 287 (1978).
[8]David Bohm and David Pines, Phys. Rev. **92**, 609 (1953).
[9]David Pines, Phys. Rev. **92**, 626 (1953).
[10]H. Suhl and N. R. Werthamer, Phys. Rev. **122**, 359 (1961).
[11]Marvin L. Cohen and Volker Heine, in *Solid State Physics*, edited by H. Ehrenreich, F. Seitz, and D. Turnbull (Academic, New York, 1980), Vol. 24, p. 37.
[12]L. J. Sham, J. Phys. Soc. Jpn. **49** Suppl. A, 69 (1980).
[13]J. A. Van Vechten and Richard M. Martin, Phys. Rev. Lett. **28**, 446 (1972).
[14]Marc Kastner and R. R. Forberg, Phys. Rev. Lett. **36**, 740 (1976).
[15]H. Wendel, Richard M. Martin, and D. J. Chadi, Phys. Rev. Lett. **38**, 656 (1977).
[16]John R. Reitz, Phys. Rev. **105**, 1233 (1957).
[17]Doris J. Olechna and Robert S. Knox, Phys. Rev. **140**, A986 (1965).
[18]W. J. Choyke and Lyle Patrick, Phys. Rev. **108**, 25 (1957).
[19]J. Treusch and R. Sandrock, Phys. Status Solidi **16**, 487 (1966).
[20]W. Kohn and N. Rostoker, Phys. Rev. **94**, 1111 (1954).
[21]Rolf Sandrock, Phys. Rev. **169**, 642 (1967).
[22]Simpei Tutihasi and Inan Chen, Phys. Rev. **158**, 623 (1967).
[23]H. J. Queisser and J. Stuke, Solid State Commun. **5**, 75 (1967).
[24]W. Henrion, Phys. Status Solidi **20**, K145 (1967).
[25]F. Urbach, Phys. Rev. **92**, 1324 (1953).
[26]Gareth G. Roberts, Simpei Tutihasi, and Richard C. Keezer, Phys. Rev. **166**, 637 (1968).
[27]G. Weiser and J. Stuke, Phys. Status Solidi B **45**, 691 (1971).
[28]W. Lingelbach, J. Stuke, G. Weiser, and J. Treusch, Phys. Rev. B **5**, 243 (1972).
[29]R. J. Elliot, Phys. Rev. **108**, 1384 (1957).
[30]Juhani von Boehm and Peter Krusius, Int. J. Quantum Chem. **8**, 395 (1974).
[31]P. Krusius, J. von Boehm, and T. Stubb, Phys. Status Solidi B **67**, 551 (1975).
[32]F. Nizzoli, Solid State Commun. **22**, 387 (1977).
[33]F. Nizzoli, J. Phys. C **11**, 673 (1978).
[34]S. F. Boys, Proc. Roy. Soc. London, Ser. A **200**, 542 (1950).
[35]Isiah Shavitt, Methods Comput. Phys. **2**, 30 (1963).
[36]Enrico Clementi and Carla Roetti, At. Data Nucl. Data Tables **14**, 177 (1974).
[37]Vinay Ambegaokar and Walter Kohn, Phys. Rev. **117**, 423 (1960).
[38]P. Bammes, R. Klucker, E. E. Koch, and T. Tuomi, Phys. Status Solidi B **49**, 561 (1972).
[39]J. Frenkel, Phys. Rev. **37**, 17 (1931).
[40]G. H. Wannier, Phys. Rev. **52**, 191 (1937).
[41]Giancarlo Baldini, Phys. Rev. **128**, 1562 (1962).
[42]R. Bonneville and G. Fishman, Phys. Rev. B **22**, 2008 (1980).
[43]J. H. Apfel and A. M. Portis, J. Phys. Chem. Solids **15**, 33 (1960).
[44]M. Balkanski and R. D. Waldron, Phys. Rev. **112**, 123 (1958).
[45]Philip W. Baumeister, Phys. Rev. **121**, 359 (1961).
[46]E. F. Gross and B. V. Novikov, J. Phys. Chem. Solids **22**, 87 (1961).